16th Australasian Fluid Mechanics Conference
Crown Plaza, Gold Coast, Australia
2-7 December 2007

Study of Underexpanded Supersonic Jets with Optical Techniques

D. Mitchell, D Honnery and J. Soria

Laboratory for Turbulence Research in Aerospace and Combustion, Dept of Mechanical Engineering Monash University, Melbourne, VIC, 3163 AUSTRALIA

Abstract

An experimental investigation of underexpanded axissymmetric supersonic jets is presented. Particle Image Velocimetry is used to obtain quantitative measurements of the velocity field, while a high framerate shadowgraph technique is used to assess shock position and stability. The PIV technique demonstrates the ability to consistently resolve the instantaneous velocity field, with major flow characteristics such as shock structures clearly evident. The shadowgraph images show that at lower pressures the shock structures are highly unstable, demonstrating periodic oscillation in angle and position, while in the highly underexpanded condition the location of the Mach disk is stable. A discussion of limitation due to optical resolution and particle fidelity is presented, concluding that the system is more limited by inadequate particle fidelity post-shock than sensor limitations.

Introduction

Supersonic free shear flows, such as circular and planar jets, have occupied the attention of researchers for over half a century. Understanding the characteristics of supersonic jets is critical to the optimization of thrust generation for rockets and gas turbines. The bulk of research in supersonic jet flows has focused on the sound generation mechanisms associated with the phenomenon of "screech", where instability waves in the jet interact with the shock cells formed due to underexpansion to create acoustic waves.

However, screech only occurs over a relatively small range of the potential operating conditions of supersonic jets. The screech phenomenon disappears at relatively low levels of underexpansion, meaning that jets at higher pressure ratios have received substantially less attention. However these high pressure ratio jets occur in many instances of both the aerospace and machining industries, and a better understanding of their physics is required.

A lack of experimental data is still evident for supersonic jets, due to the inherent difficulties in obtaining measurements in supersonic free shear flows. The use of any form of intrusive probe is rendered difficult due to the speed at which the fluid is moving; any solid obstacle in the flow will induce a normal shockwave and fundamentally alter the flow. This means only optical or acoustic techniques offer any hope of producing valid measurements. Acoustic techniques have been used extensively in the measurement of screech, however the information they provide about the flow field is very limited. This leaves optical techniques as the only viable means of obtaining the majority of the data required to characterize the flow. A number of optical techniques are available that are capable of measuring various fluid properties such as velocity, pressure, temperature, and scalar transport.

Velocity measurements have been taken via Particle Image Velocimetry (see: [27], [1], [10], [3]), Laser Doppler Velocimetry (see: [5], [4]), and Spectrally Resolved Rayleigh Scattering (see [16]). Qualitative visualization, and identification of shock locations has been performed by authors too numerous to list

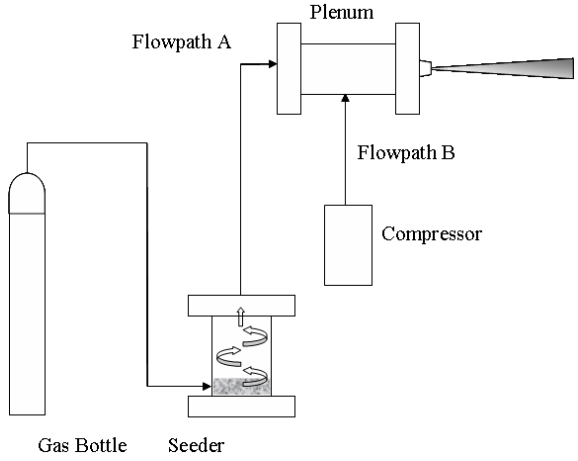

Figure 1: Experimental Facility

over the last fifty years, using techniques such as shadowgraphs and Schlieren. Quantitative measurement of flow scalars such as density and temperature are also beginning to emerge, using techniques such as Spectrally Resolved Rayleigh Scattering (again see [16]), and Background Oriented Schlieren (see [24]). Due to the inherent difficulties in implementing even optical techniques, the majority of these measurements are limited to mean-field studies, with instantaneous velocity fluctuations proving too challenging to measure. Some studies such as [17] have been able to produce high sampling rate measurements, however these are at a single point rather than in a plane.

Experimental Methodology

The experiments described herein were conducted in the Laboratory for Turbulence Research in Aerospace and Combustion Supersonic Jet Facility. A schematic of the facility is provided in Figure 1. The Jet Facility was fitted with a 5mm converging nozzle. Air was supplied to the plenum chamber via two flowpaths, denoted A and B. A compressed air line from a factory compressor was used to supply the plenum via flowpath A, while flowpath B was supplied from compressed gas cylinders via a seeding device. Valves on both inlets allowed the contribution from each flowpath to be balanced to obtain optimal seeding density. After the seeded and unseeded air streams mixed inside the plenum, they were accelerated through the converging nozzle to sonic velocities. The jet was situated within a glass cage to minimize contamination of the laboratory space by seed particles. The edges of the cage were 30 nozzle diameters from the jet centreline. Only the nearfield of the jet was investigated, i.e. from 0-10 nozzle diameters.

Measurement Technique - Particle Image Velocimetry

Particle Image Velocimetry is a well established optical technique capable of obtaining planar-field 2-component velocity information from a flow. Its non-intrusive nature makes it ideal

for measurements in supersonic flows, though the requirement for the introduction of solid seeding particles into the flow can be problematic. The Multigrid Cross-Correlation Digital Particle Image Velocimetry (MCCDPIV) algorithm for analysing the image pairs is described in [22]. It utilizes an adaptive based on the principle that the locations of the interrogation windows in the two images of the pair do not necessarily have to coincide. By obtaining a local velocity estimate using a large interrogation window, the second interrogation window can be displaced by converting this velocity estimate into a displacement. This displacement effectively increases the measurable dynamic range of velocity and reduces the uncertainty of the measurement. This is advantageous when examining high speed flows, where the high particle displacements may necessitate the use of large interrogation windows, and large velocity gradients may be present.

A PCO 4000 camera mounted orthogonal to the jet, with an array size of 4008x2760 pixels was used to image the flow. To improve the framerate to 0.5Hz the region of interest was reduced to 4008x1800 pixels. The camera is fitted with a 105mm Micro Nikkor Nikon lens set at an aperture of $f5.6$, and a 25mm spacer to increase the magnification of the system. Particles within the flow were illuminated by a laser sheet generated from a Nd:YAG laser at 532nm wavelength, with 80mJ pulse energy.

The high resolution of the PCO 4000 allows this study to be conducted at a significantly higher spatial resolution than some previous studies in this area. Unfortunately this is somewhat offset by the substantially smaller jet diameter, meaning the gain in resolution relative to the scale of structures in the flow is reduced. It is difficult to provide a direct comparison as many previous studies have not provided sufficient information to determine the spatial resolution of their measurements. As a point of comparison, [3] conducted a series of PIV measurements with a spatial resolution of 130μm/px, whereas the current study has a spatial resolution of 10.7μm/px. However the nozzle used in the work of [3] had a diameter of 25mm, whereas the present study utilizes a nozzle of only 5mm diameter. Thus in non-dimensional terms, the spatial resolution based on final interrogation window size was 0.17d for the work of Chauveau et al, and 0.07d for the present study. These experimental parameters are presented in Tables 1 and 2.

Parameter	Value
Optical Magnification	0.84
Magnification [px/μm]	0.09
Spatial Resolution [μm/px]	10.71
δt	480ns
Fstop	5.6
Pixel Size	9μm
Array Size	36.1mm x 16.2mm
Velocity Dynamic Range	61.8dB

Table 1: Optical Parameters

Parameter	Value	Non-Dimensional Value
IW_0	96px	0.21d
IW_1	32px	0.07d
Grid Spacing	16px	0.03d
Depth of Field	0.4mm	0.08d

Table 2: Non-dimensional PIV Parameters

Flow Seeding

The selection of an appropriate seed material is important in all PIV studies, however it is of critical importance when considering supersonic flows. Large velocity gradients, particularly due to shockwaves, mean only the very smallest particles will follow the flow faithfully. Variations in density within the flow will also result in non-uniform distribution of particles within the flow ([23]). However, Urban and Mungal cite [18] as demonstrating that "particles need only track the velocity variations from one PIV interrogation region to another, and that velocities along gradients too steep for the particles to follow will nevertheless be reflected faithfully in the average values reported for their interrogation region". Therefore one should endeavour to ensure that particles will respond to steep velocity gradients sufficiently quickly as to accurately represent the spatial average velocity for a given interrogation window. However with the constant improvement of available resolution on CCD arrays, as well as the limitations imposed by other particle selection criteria, this may not always be feasible.

The most significant velocity gradients in underexpanded jets are those caused by the strong normal shocks in the core flow of strongly underexpanded jets, and to a lesser extent the weak oblique shocks present in both strongly and weakly underexpanded jets. A shockwave is a discontinuity in the flow, often only several microns across, which is well below the resolution of current PIV systems. Shockwaves represent a step decrease in flow velocity, and the response of seed particles to this step decrease must be quantified.

The characteristic equations for particle response to shocks as detailed in [23], as well as [12] and [11], are presented here. Melling specifies that the standard methodology for quantifying particle response is particle relaxation time, denoted τ_t. Particle relaxation time is defined as the time after a step change in flow velocity required for the velocity lag $|\hat{V}| = |\hat{U}_P - \hat{U}_F|$ to be reduced by a factor of $\frac{1}{e} = 0.368$, Melling provides the basic equation from which the particle relaxation time is to be estimated, stating that empirical estimates of the drag coefficient for the particles are required. [23] conducted an extensive investigation into the behaviour of particles across oblique shocks, taking from [12] a definition for the drag coefficient of

$$C_D = \frac{24}{Re_D(1+2.7Kn_d)} \tag{1}$$

Here Kn is the Knudsen number, determined by the ratio of the mean free path of the gas l to the particle diameter:

$$Kn = \frac{l}{d_P} \tag{2}$$

The Knudsen number is included as a correction for the fact that continuum assumptions are somewhat tenuous for sufficiently small particles. Both theoretical and experimental investigations have shown that the resistance of a particle to flow decreases as the Knudsen number increases ([19].

Thus from the drag coefficient in Equation 1, the particle relaxation time can be expressed as:

$$\tau_p = \frac{\rho_p d_p^2}{18\mu}(1+2.7Kn_d) \tag{3}$$

Equation 3 demonstrates that particle response depends on both particle and fluid characteristics. As the fluid characteristics will be defined by the flow in question, only particle density and diameter can be varied by the user. Ideally both should be minimized to achieve an optimal relaxation time, however in practice there are limits on both parameters. Density will be determined simply by the material available, while minimum possible diameter will be defined by both the powder type and the optical limits of the system.

To calculate the mean free path, we refer to kinetic gas theory:

$$\lambda = \frac{RT}{\sqrt{2}\pi d_a^2 N_A P} \tag{4}$$

Here N_A is Avagadros number, d_a is the diameter of a typical air molecule. Temperature variation is neglected as trivial compared to other terms, and the nominal diameter of air is taken as 3 angstroms. Taking the stagnation pressure in the plenum (a maximum of 500kPa for this study) and the atmospheric pressure as the upper and lower bounds yields a mean free path ranging between 2×10^{-8} and 1×10^{-7} for the flow conditions considered.

Here pigment grade titanium dioxide (TiO_2) was used. Previous studies have used silica dioxide ([3], [27]) aluminium oxide ([21], [13]), olive oil ([10], [14]), as well as TiO_2 ([9], [23]).

The pigment grade TiO_2 has a nominal particle diameter specified by the manufacturer of 0.4μm, however no information about the range of sizes is provided. A better knowledge of particle geometry was necessary if a precise estimate of relaxation time was to be made. The TiO_2 particle size distribution, surface area moment mean (D[3,2]) and the mass moment mean (D[4,3]) were determined using a Mastersizer 2000 (Malvern Instruments Ltd, UK), employing a Scirocco dry powder feeder. The particle feed rate was controlled using the variable feed-rate vibrating tray whilst dispersion was achieved by accelerating particles within a compressed air stream, together with particle and wall collision.

Figure 2 shows the particle size distributions for two samples of the TiO_2. One sample was taken of particles and agglomerates. The size distribution for this sample was bimodal, with peaks at $0.52\mu m$ and $75\mu m$. This suggests the bulk of the agglomerates are on the order of 150 times larger than the individual particle sizes. A second sample was taken without agglomerates to provide statistics on the individual particle size. The median measured particle diameter without agglomerates was $0.56\mu m$, with a span of $1.032\mu m$. 10 percent of particles have a diameter below $0.33\mu m$ and 90 percent have a diameter below $0.88\mu m$.

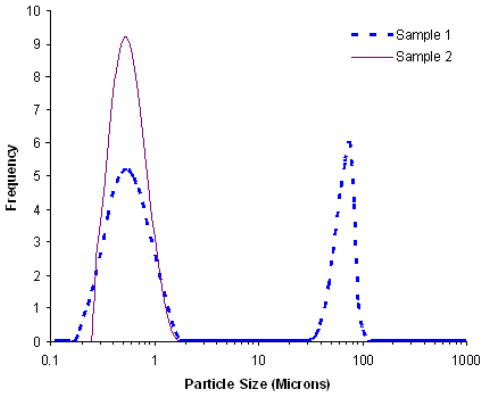

Figure 2: Particle size distribution for TiO_2 sample

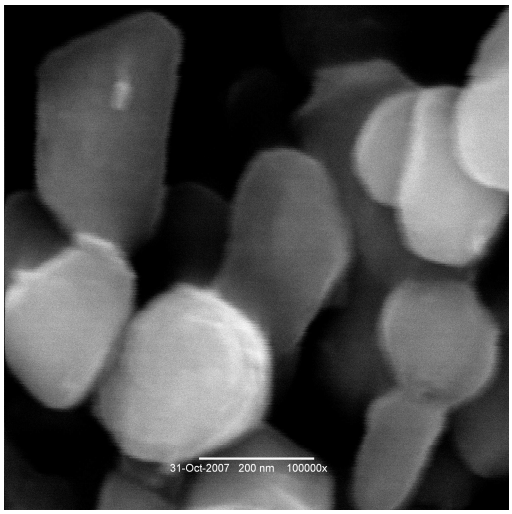

Figure 3: Particle size distribution for TiO_2 sample

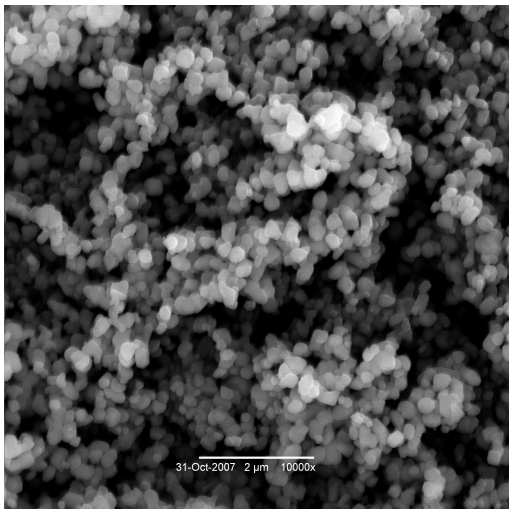

Figure 4: Particle size distribution for TiO_2 sample

Thus an approximate relaxation time based on mean particle diameter can be calculated, as well as relaxation times based on agglomerate size, as well as upper and lower percentile bounds.

Depending on the local pressure, particles with a mean diameter of $0.55\mu m$ will experience a particle relaxation time of between 4 and 6 μs. At a velocity of $550ms^{-1}$, which corresponds to the ideally-expanded velocity for a 500kPa reservoir, particles will move between 2 and 3mm in this time, which in non-dimensional terms is 0.4d-0.6d. Particles in the tenth percentile at $0.33\mu m$, will experience a maximum particle relaxation time of 1.5-2.5μm depending on flow conditions, corresponding to a relaxation distance of 0.2-0.25d. In the 90th percentile, the maximum relaxation time will be 10-13μm, with a relaxation distance of approximately 1.2d. The relaxation time of the agglomerates is not worth considering, as they will leave the measurement region before attaining anything close to the correct velocity.

Referring to Table 1, the spatial resolution based on final window size is 0.07d. For our system to be sensor-limited rather than particle-limited, our particles would have to achieve their "true" velocity within a single interrogation region. It is evident from the above calculations that will not be the case, even for particles in the tenth percentile. Consequently in the region following the Mach disk, particle lag effects will play a far greater role than sensor constraints in limiting the faithfulness of the returned velocities. The substantial variation in relaxation distance across the span of the distribution also reduces confidence in the measurement downstream of shocks.

The variation in particle size across the distribution will also introduce bias errors in the post-shock region. The variation in response to the shock will result in a non uniform displacement of the particles, despite the actual fluid velocity being constant. This will result in reduced displacement-correlation peaks ([25]

Figures 3 and 4 show scanning electron microscope (SEM) images of the TiO2 powder. In addition to the equivalent diameter of the individual particles, the shape is also of interest. Particle Image Velocimetry is based on the recording of light reflected by Mie Scattering. Mie theory assumes spherical particles, however as the images demonstrate the shapes of the particles are quite irregular. This can have a significant impact on the ability of the PIV technique to faithfully resolve the flow. As particles of irregular shape move through the flow, they will experience rotation as well as translation. Thus the cross section presented to the incident light sheet will vary from moment to moment. This can mean a particle will return a large amount of scattered light in one image of a pair, but not in the next. This reduces the strength of the correlation peak, and thus the ability of the PIV system to faithfully resolve the flow.

Seeding Apparatus

In addition to the importance of selecting an appropriate seed material, a method for seeding the fluid flow is required. A number of different approaches are available, as detailed in [12]. Previous work by the authors used a cyclonic seeder design [13] based on the work of [8], a Laskin droplet generator [15], and a cyclonic seeder based on the design of [3]. The current design utilizes a hybrid fluidized bed / cyclone system, with the tangential air injection point at the bottom of the powder bed. The seeding level produced by this device was substantially more stable than the previous pure cyclone system, though still far from ideal.

Measurement Technique - Shadowgraph

Shadowgraph techniques have been in use for several hundred years, and in the last century have been a popular method of visualizing shock structures in compressible flow. Shadowgraphs are less sensitive to density gradients than their Schlieren counterparts, however strong gradients such as those generated by shock structures are clearly resolved.

In the present suite of experiments, a Shimadzu Hypervision camera capable of acquiring images at a framerate of 1MHz has been used to acquire shadowgraph images. This exceptionally high framerate allows for examination of time resolved evolution of shock structure within the jet. Light is provided by a CREE XRE-Lamp LED producing 110 lumens of light. This light is collimated through a pair of 100mm diameter lenses and projected through the jet directly onto the CCD array. Supply of light was constant, with no pulsation or triggering.

The sharpness of the images is limited by the distance between the jet and the CCD array. While this has been reduced as much as experimental geometry allows, sensitivity and image sharpness are reduced by distance, a "'contact"' shadowgraph being the optimal case.

Shadowgraph images were acquired here at a framerate of 500kHz. Each image had an exposure time of 0.5μ s, and sequences of 100 images were acquired, with camera gain set at 30x.

Results

Axisymmetric Free Jet - PIV

A typical raw PIV image of the jet operating at a nozzle pressure ratio (NPR) of 2.5 is displayed in Figure 5. This is a double exposed image of the Mie scattering from the seed particles in the flow. The immediate expansion following exit from the nozzle is evident, as is a bright region corresponding to the first Mach disk. Though the lack of freestream seeding makes structures in the shear layer less clear, turbulent breakup via Kelvin-Helmholtz instabilities are still evident some distance downstream of the Mach disk. While the clear evidence of the Mach disk in the raw PIV image is helpful as a flow visualization, it is also demonstrative of variation in fluid density resulting in variation of seed density. This makes optimizing seed density in the flow difficult, making the extraction of velocity information via PIV more challenging.

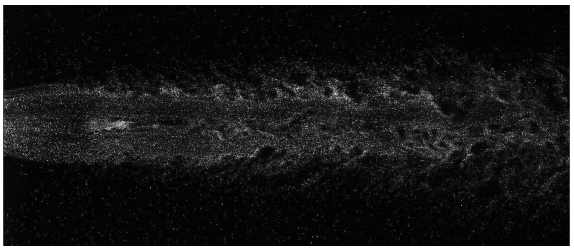

Figure 5: Raw PIV image for NPR=2.5

Weakly Underexpanded Jets

Jets in the weakly underexpanded condition, with NPR ranging from 1 to 1.85 were examined. Pressure ratio was determined by measuring stagnation pressure via a transducer, then calculating critical pressure using basic isentropic relations. Mean samples for each jet are taken over 184 image pairs. The number of image pairs was dictated by the available buffer on the camera. The entrainment field was not seeded during these experiments, which meant that seed density was at times too low for the PIV algorithm to extract velocity data in the shear

Jet NPR	M1/M2	Shock Spacing (x/d)	Last Shock (x/d)
1.3	1.03	0.5	1.5
1.6	1.11	1	3
1.85	1.2	1.3	6

Table 3: Weakly underexpanded jet shock structures

layer. Turbulent structures in the shear layer were still evident in the instantaneous realizations, however the number of rejected vectors was higher than in the core of the jet. All velocities shown are normalized against the theoretical nozzle exit velocity, where the flow is sonic at $315ms^{-1}$, due to the difficulties of taking measurements exactly at the nozzle exit.

The first jet considered is nominally in the ideally expanded condition, at NPR=1. However examination of the exit velocities suggest that the jet is actually a subsonic jet at M=0.9.

As expected, there is no evidence of shocks when NPR=1. However, as the back pressure is increased, shocks are immediately evident in the flow. This is evident in the oscillation of velocity observed in Figure 7, where mean centreline velocities for the jets are plotted at various pressure ratios.

As the back pressure increases, so too does the strength of the shocks, and at NPR=1.85, the shocks begin to take on appreciable curvature immediately following exit from the nozzle as depicted in Figure 6. This curvature indicates an approach to the strongly underexpanded region defined as NPR > 2.0, as detailed in [6]. This transition to the strongly underexpanded condition occurs when the initial expansion from the nozzle exit becomes sufficiently high that recompression cannot be achieved in the conical "cell" bounded by the oblique incident shocks from the nozzle lip. At this transition point, the pressure differential becomes sufficiently high that a normal shock is required to achieve the necessary level of recompression.

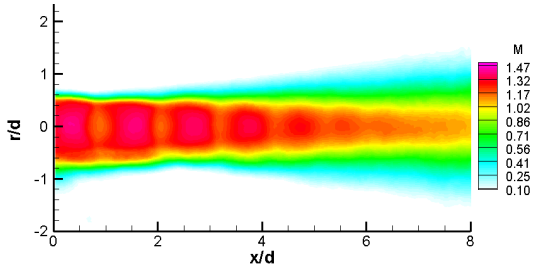

Figure 6: Mean normalized velocity contour for NPR=1.85 taken over 184 images.

The centreline velocities for the four weakly underexpanded jets are plotted in Figure 7. The increasing strength of the shocks with increasing NPR is evident from the greater magnitude of oscillation in the centreline velocity for the NPR=1.85 jet. The influence of pressure ratio on shock spacing is also evident. The jet at NPR=1.3 has the highest frequency oscillation of velocity, while the shocks for NPR=1.85 are much more widely spaced. Figure 7 also shows that the shock train decays faster for jets at lower pressure ratios. Approximate values of these three characteristics of the shock structure are presented in Table 3. The location of the termination of the shock train is simply defined here as the point at which no further periodic oscillation is observed.

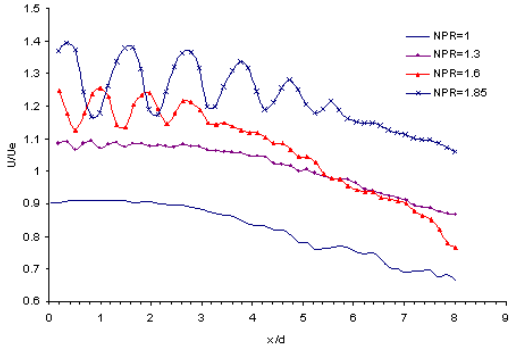

Figure 7: Centreline normalized velocity for weakly underexpanded jets.

The RMS velocities along the centreline of the four jets are plotted in Figure 8 to examine the influence of shock structures on velocity fluctuations. The range considered here is from 0 to 4 x/d to improve clarity. There are four possible primary sources of variation in the recorded RMS values. The first potential cause is variation in the velocity amplitude, caused by variation in shock strength. The second is variation in velocity phase, caused by variation in shock location. The third is noise in the data (either amplitude or phase) due to the failure of the PIV algorithm to accurately construct the velocity field from the recorded images. The fourth possible source of variation is particle biasing effects downstream of the shock. Moment to moment variation in particle distribution in the flow may result in a variation in particle relaxation time downstream of the shocks, meaning each instantaneous data point will have a different level of "smearing" in the post-shock region. It is difficult to ascertain from Figure 8 which effects are dominant. The case of NPR=1 is useful as a baseline, as there are no shock effects, and any RMS variation is simply due to fluctuations in the jet and in the PIV process. There is a very slight periodic oscillation in the RMS with varying x/d for the underexpanded jets that is not evident for the NPR=1 jet which may be due to the influence of the shocks. The RMS velocities in the initial core region of the jet are very low, and increase as the fluid moves downstream. This increase is to be expected if the primary source of RMS variation is fluctuations within the jet itself, rather than fluctuations induced by experimental error.

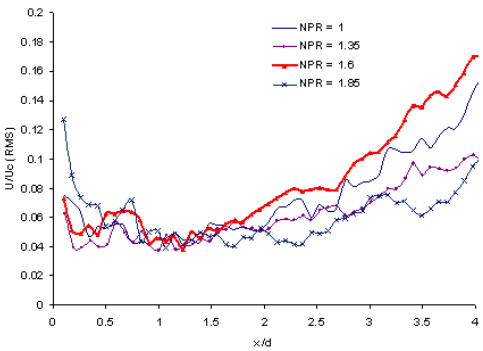

Figure 8: Centreline normalized RMS velocity U/Ue for weakly underexpanded jets.

Strongly Underexpanded Jets

Figure 9 shows a mean velocity field for the jet at NPR=2.5. The Mach disk in the core of the flow is evident at the point where velocity in the core begins to decline at x/d = 1.2. The minimum velocity does not occur until approximately x/d = 1.5. This delay in the occurrence of minimum velocity is due to particle lag effects. The relaxation distance of 0.3d is actually slightly below the values predicted by theory earlier. While the equations used for particle relaxation are typically considered on the conservative side ([12], it may also be that the exact location of the Mach disk is slightly further upstream than the observed point where velocity initially declines. The effects of oblique shocks between the Mach disk and the jet core are also visible, extending forwards at an angle from the Mach disk to the jet boundary. The structure of the velocity field that can be determined from the PIV measurements is in accordance with the theoretical work of [6] as well as the experimental findings of studies such as [27].

Examination of the raw PIV image presented earlier shows a region of high seed density at the location of the Mach disk. To ascertain the effect this may have on the prediction of local velocity, the mean velocity field is examined in more detail. For the purposes of this brief examination, the jet is assumed to be isothermal. While in practice this will not be true, the sound-speed variation is assumed to be sufficiently small as to be negligible. Mach numbers upstream and downstream of the Mach disk can then be calculated for the mean field, yielding values of 1.5 and 0.4 respectively. From the normal shock relations ([2]), for an upstream Mach number of 1.5, the Mach number downstream of a normal shock should be 0.7. Examination of the instantaneous images reveals a similar discrepancy. It is suggested that the variation in seed density due to local fluid density variation is resulting in an underprediction of the velocity in the region a short distance downstream of the Mach disk.

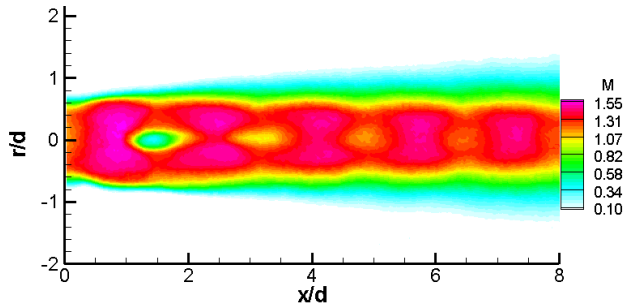

Figure 9: Mean normalized velocity contour field for jet at NPR=2.5 taken over 92 images.

Axisymmetric Free Jet - Shadowgraph

Sample shadowgraphs are supplied for the weakly underexpanded case in Figure 10 and for the strongly underexpanded case in Figure 11. For the weakly underexpanded case, oscillation of the shocks immediately following the nozzle exit was evident. A flapping motion from left to right in the image was evident, with the angles of the two oblique shocks varying.

For the strongly underexpanded case, no motion in the location of the Mach disk was evident. At this pressure ratio the first Mach disk is sufficiently strong that the flow remains subsonic downstream of it, rather than returning to supersonic conditions as seen in the PIV of the NPR=2.5 jet.

The oscillations evident in the weakly underexpanded case are of particular interest in reference to the RMS values obtained from the PIV measurements. The variation in angle and position will result in both phase and amplitude variation in the RMS values. Thus for the weakly underexpanded cases, the influence of shock oscillation on the PIV results will be significant. While this could potentially be addressed through phase locking, this would require the use of acoustic sensors, and significant additional experimental complexity.

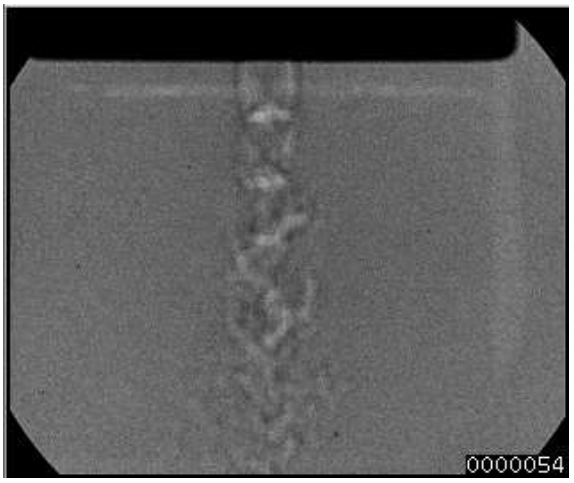

Figure 10: Shadowgraph for underexpanded jet at NPR=1.5

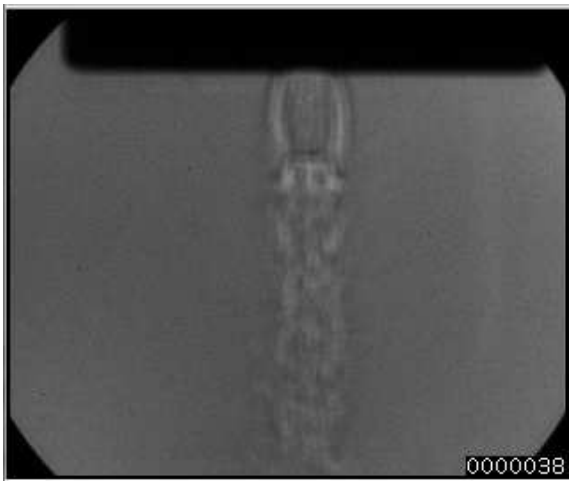

Figure 11: Shadowgraph for underexpanded jet at NPR=7

Future Considerations

The PIV measurements and theoretical calculations herein both suggest that the measurements are primarily particle-limited rather than sensor-limited. Using the current optical system and holding all other parameters constant, to reduce the particle-lag below the spatial resolution limit of 0.07d would require a TiO_2 particle with a diameter of $0.2\mu m$. This is certainly attainable, as the literature describes TiO_2 particles with nominal diameters of $0.015\mu m$ ([23] and [26]), as well as other metal powders with diameters measured on the order of several nanometers ([9] [3]. However these are nominal particle sizes, and agglomeration must be accounted for. Methods of dealing with agglomeration are described in the literature such as the use of cyclonic separators ([3]) and shearing nozzles ([9]), and these may prove suf-

ficient to keep the mean particle diameter low enough that resolution ceases to be particle-limited. Only once this is achieved can the true benefits of high resolution CCD arrays such as the PCO 4000 be fully realized for supersonic flows. It should also be noted that the influence of particle fidelity varies inversely with nozzle geometry. Structures such as shocks scale based on nozzle diameter, as diameter is increased, the size and spacing of shocks increases accordingly. Particle response time is unaffected by experimental geometry, thus a larger nozzle would mean an improved response in non dimensional terms.

The variation of seeding density with local fluid density is also evidently a potential problem. This is not a new concern, and some literature exists regarding potential solutions ([20]), however further research will be devoted to this area. The link between fluid density and particle concentration offers a useful tool for planar visualization of density gradients, as detailed in [7], however it is potentially limiting when attempting to extract velocity information.

Conclusions

A series of high spatial-resolution measurements have been taken in underexpanded jets in both the weakly and strongly underexpanded condition. Local structure was resolved in both the instantaneous and mean fields. The resolution of the measurements in the region around the normal shocks was demonstrated to be particle-limited rather than sensor-limited. Obtaining a steady level of flow seeding with minimal agglomeration continued to prove the principal challenge in supersonic free shear flows.

Acknowledgments

The authors would like to acknowledge the assistance of several people who made this research possible. Mr Ivor Little for his technical expertise and tireless efforts in the design and manufacture of the experimental apparatus. Dr Xian Wang for his assistance with particle fluidization techniques. Dr Gareth Forde for his very generous work with the particle sizing analysis, in both the data collection and analysis stages. Mr Michael Mitchell for his assistance in the laboratory, and Mr Callum Atkinson, Dr Chong Wong and Ms. Sophie Herpin for their general assistance. The financial support of the Australian Research Council is also gratefully acknowledged.

References

[1] Alvi, F., Ladd, J. and Bower, W., Experimental and computational investigation of supersonic impinging jets, *AIAA Journal*, **40**, 2002, 599–608.

[2] Anderson, J. D., *Fundamentals of Aerodynamics*, McGraw Hill, 2007.

[3] Chauveau, C., Davidenko, D., Sarh, B., Gokalp, I., Avrashkov, V. and Fabre, C., Piv measurements in an underexpanded hot free jet, in *13th International Symposium on the Application of Laser Techniques to Fluids Mechanics, Lisbon, Portugal*, 2006.

[4] Clancy, P. and Samimy, M., Two-component laser doppler velocimetry in high speed flows, *AIAA Journal*, **35**, 1997, 1729–1738.

[5] Clancy, P., Samimy, M. and Erskine, W., Planar doppler velocimetry: Three-component velocimetry in supersonic jets, *AIAA Journal*, **37 n 6**, 1999, 700–707.

[6] Donaldson, C. and Snedeker, R., A study of free jet impingement. part 1. mean properties of free and impinging jets, *Journal of Fluid Mechanics*, **45 n 2**, 1971, 281–319.

[7] Gawehn, T. and Schodl, R., Tracer based shock visualization - a new measurement technique, in *Proc. 13th International Symposium on the Applications of Laser Techniques to Fluid Mechanics, Lisbon, Portugal*, 2006, 37.3, 37.3.

[8] Glass, M. and Kennedy, I., An improved seeding method for high temperature laser doppler velocimetry, *Combustion and Flame*, **29**, 1977, 333–335.

[9] Goyne, C., Rodriguez, C., Krauss, R., McDaniel, J. and McClinton, C., Experimental and numerical study of a dual-mode scramjet combustor, *Journal of Propulsion and Power*, **v22, no 3**, 2006, 481–489.

[10] Krothapalli, A., Rajkuperan, E., Alvi, F. and Lourenco, L., Flow field and noise characteristics of a supersonic impinging jet, *J. Fluid Mech.*, **392**, 1999, 155–181.

[11] Melling, A., Tracer particles and seeding for particle image velocimetry., *Meas. Sci. Technol.*, **8**, 1986, 1406–1416.

[12] Melling, A., Tracer particles and seeding for particle image velocimetry., *Meas. Sci. Technol.*, **8**, 1997, 1406–1416.

[13] Mitchell, D., Honnery, D. and Soria, J., Particle image velocimetry measurements in an underexpanded supersonic jet, in *Fourth Australian Conference on Laser Diagnostics in Fluid Mechanics and Combustion, Adelaide Australia*, 2005.

[14] Mitchell, D., Honnery, D. and Soria, J., Optical measurements in free and impinging supersonic jets, in *13th International Symposium on the Application of Laser Techniques to Fluid Mechanics, Lisbon, Portugal*, 2006.

[15] Mitchell, D., Honnery, D. and Soria, J., Particle image velocimetry measurements and cfd analysis of an underexpanded supersonic jet, in *13th International Heat Transfer Conference, Sydney, Australia*, 2006.

[16] Panda, J. and Seasholtz, R., Velocity and temperature measurement in supersonic free jets using spectrally resolved rayleigh scattering, in *37th Aerospace Sciences Meeting and Exhibit sponsored by the American Institute of Aeronautics and Astronautics Reno, Nevada, January 1114*, 1999, volume 29, 333–335, 333–335.

[17] Panda, J. and Seasholtz, R., Experimental investigation of reynolds and favre averaging in high-speed jets, *AIAA Journal*, **44, n 9**, 2006, 1952–1959.

[18] Raffel, M., Hofer, H., Kost, F., Willert, C. and Kompenhans, J., Experimental aspects of piv measurements of transonic flow fields at a trailing edge model of a turbine blade., in *8th International Symposium on the Application of Laser Techniques to Fluids Mechanics, Lisbon, Portugal*, 1996.

[19] Rumpf, H., *Particle Technology*, Chapman and Hall, 1990.

[20] Scarano, F., Piv image analysis for compressible turbulent flows., *Advanced measurement techniques for supersonic flows. Lecture Series - von Karman Institute*.

[21] Scarano, F. and Haertig, J., Application of non-isotropic resolution piv to supersonic and hypersonic flows, in *5th International Symposium on Particle Image Velocimetry, Busan, Korea*, 2003.

[22] Soria, J., Multigrid approach to cross-correlation digital piv and hpiv analysis, in *13th Australasian Fluid Mechanics Conference, Monash University, Melbourne*, 1998, 381–384, 381–384.

[23] Urban and Mungal, G., Planar velocity measurements in compressible mixing layers, *Journal of Fluid Mechanics*, **431**, 2001, 189–222.

[24] Venkatakrishnan, L., Density measurement in an axisymmetric underexpanded jet by background oriented schlieren technique, *AIAA Journal*, **43 n 7**, 2005, 1574–1579.

[25] Westerwheel, J., On velocity gradients in piv interrogation, in *Proc. 7th International Symposium on the Applications on Particle Image Velocimetry, Rome, Italy*, 2007.

[26] Xu, J., Lin, C., Sha., J. and Zhang, K., A piv study and numerical simulation of overexpanded supersonic impinging free jet., in *14th AIAA/AHI International Space Planes and Hypersonics Systems Conference, Canberra Australia*, 2006.

[27] Yuceil, K., Otugen, M. and Arik, E., Underexpanded sonic jets, a piv study, in *Proc. 10th International Symposium on the Applications of Laser Techniques to Fluid Mechanics, Lisbon, Portugal*, 2000, 8.6, 8.6.